Materials and Design 192 (2020) 108705

Contents lists available at ScienceDirect

Materials and Design

journal homepage: www.elsevier.com/locate/matdes

Classification of mechanism of reinforcement in the fiber-matrix interface: Application of Machine Learning on nanoindentation data

Georgios Konstantopoulos [a], Elias P. Koumoulos [a,b,*], Costas A. Charitidis [a]

[a] RNANO Lab—Research Unit of Advanced, Composite, Nano Materials & Nanotechnology, School of Chemical Engineering, National Technical University of Athens, GR-15773 Zographos Athens, Greece

[b] Innovation in Research & Engineering Solutions (IRES), Boulevard Edmond Machtens 79/22, 1080 Brussels, Belgium

HIGHLIGHTS

- Artificial Intelligence (AI) identified the interface reinforcement in CFRPs.
- Support Vector Machines performed well in both testing and validation of the model.
- Functionalization on CFs was predicted with F1-score equal to 65% and accuracy 67%.
- Model was validated at different nanoindentation depth with accuracy 72.7%.
- Feedback from AI could enhance materials design, decision-making, and quality control.

GRAPHICAL ABSTRACT

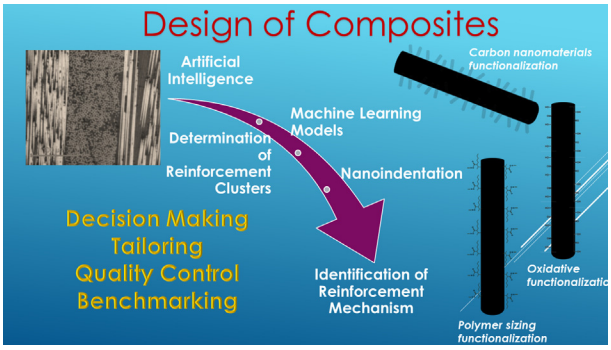

ARTICLE INFO

Article history:
Received 8 January 2020
Received in revised form 26 March 2020
Accepted 29 March 2020
Available online 3 April 2020

Keywords:
Artificial intelligence
Machine Learning
Nanoindentation
Interface
Carbon fiber reinforced composites
Multiclass classification

ABSTRACT

Carbon fiber reinforced polymer manufacturing is emerging, with multiple studies to focus on the design of interfacial reinforcement to ensure the maximum of composite properties, but also respectively to be able to align with zero defect manufacturing. The controversy on the engineering approach is a data-driven task that can be efficiently tackled by involving Artificial Intelligence in order to establish unbiased structure-property relations. In the present study, nanoindentation mapping data were processed with Machine Learning classification models to identify the interfacial reinforcement. The data preparation included normalization and sorting out of highly similar data with k-means clustering, since nanoindentation on epoxy matrix does not enhance insight on the mechanism of reinforcement. The trained models included neural networks, classification trees, and support vector machines. Realization of models' performance was evaluated on the test dataset as screening to obtain best fitted models for each algorithm. Transfer learning potential was demonstrated by extrapolating the prediction of best trained models to a validation dataset at different indentation depth with support vector machines outperforming the other models. Overall accuracy was 67% on the test dataset, F1 Score was 65% in the prediction of reinforcement mechanism classes and 72% in case of pristine specimen, while accuracy on validation dataset was 72.7%. Prediction metrics were comparable to other case studies of real-world classification problems. Computational time-cost for tuning and training was sustainable and equal to 2.3 min.

* Corresponding author at: RNANO Lab—Research Unit of Advanced, Composite, Nano Materials & Nanotechnology, School of Chemical Engineering, National Technical University of Athens, GR-15773 Zographos Athens, Greece.
E-mail addresses: epk@innovation-res.eu, elikoum@chemeng.ntua.gr (E.P. Koumoulos).

https://doi.org/10.1016/j.matdes.2020.108705

1. Introduction

Carbon fiber reinforced polymers (CFRPs) are few steps from commercialization to significantly substitute metal components in aerospace, automotive, construction fields [1–3]. Since their delamination and degradation mechanisms are extensively studied, several modifications of carbon fibers (CFs) surface chemistry have been applied to enhance composites' performance, through effective transfer loading for matrix to fibers [4–8]. Functionalization improves the wetting of epoxy and CFs interface in order to achieve robust mechanical performance and enhance ageing resistance by even improving mechanical integrity [8]. Industrial-friendly technologies such as plasma oxidation improve chemical bonding, while deposition of thin polymeric films has also been involved to improve chemical affinity between matrix and CFs [9,10]. Another innovative engineering approach is the incorporation of carbon-based nanomaterials on CFs surface in order to improve adhesion with matrix phase [11,12]. These modifications have provided improvement in composite performance by integrating a different mechanism of reinforcement in each case and have the potential to be employed continuously in larger scale.

However, in order to engineer a CFRP tailored towards a specific application, there is the need to understand intrinsic differences between modifications. Differences are recognized in molecular weight, chemical nature of functional groups and of their core, which is organic in case of polymers and inorganic in case of nanomaterials. Moreover, in case of nanomaterials properties such as aspect ratio, geometry, and diameter could significantly alter the interfacial properties of CFRPs [11,12]. Similar to recently developed ontology databases [13,14], recognition of reinforcement mechanism can assist the development of materials characterization databases and ontologies (*CHADA*, case study of Nanoindentation) [15].These alterations influence changes in mechanical properties and are highly considered in materials design, since there is high industrial competitiveness. Artificial Intelligence (AI) and Machine Learning (ML) are the next step in materials informatics towards smartization [16] and is expected to be hugely involved in the ongoing *4.0 (fourth) Industrial Revolution* [17]. Data analysis till recently was implemented through statistical models for industrial process control [17], which meets a threshold of information feedback, which ML overcomes by taking advantage of increased computational power and multidimensional patterning. Considering recent proceedings with high speed nanoindentation and generation of thousands of data at short periods of time [18,19], ML can contribute to establishment of unbiased structural-property relations in materials science [14–16,20–24], to correlate the chemistry involved during processing to the resultant mechanical properties; feedback from ML creates new opportunities in product or process design with better decision support [17,25–28]. Classification in construction and materials industries is both data- and product-driven [29,30], and is mainly focused in production planning and quality control [16,17]. Moreover, ML tasks can support the identification of a composite structure fingerprint, which is theoretically correlated to the nature of reinforcement. These tasks are of great importance in order to standardize an industrial manufacturing plant and achieve fast transfer of a laboratory idea into industrial production and applications [17], to perform real-time characterization [24] for fault/anomaly detection [16,17,25,30] and components benchmarking [17,30].

Nowadays there is a wide range of ML algorithms available to deal with real-world classification tasks. These algorithms can be hierarchical (for instance decision trees [31]), which require less data cleaning [27] and classification process is more straightforward [32]. Another category of ML are black box models, such as support vector machines (SVM) and artificial neural networks (ANN), which can identify unseen and complex patterns and be highly accurate [26,32,33]. Especially, ANNs such as multi-layer perceptron (MLP) do not require special treatment of data, due to their efficiency in classification of both categorical and numerical data [29]. An ANN introduces adaptive weights to establish connections between (hidden) layers [33]; however a huge amount of data should be provided to enhance prediction metrics [27]. SVMs are memory efficient [27], but suffer in presence of noisy data [26]. SVMs accept only numerical input to map high dimensional data by using the kernel functionality to separate classes with hyperplanes introduction [17,33]. A prominent and easily deployable classification tree algorithm is C5.0, which has gained industrial appeal since it can be as efficient as black box methods [32]. Another useful algorithm is Adaptive Boosting (AdaBoost), which includes weaker learners and improves them (boosting process), and finally filters the relevant features that improve the model predictions by reducing biased errors [31,33]. Extreme gradient boosting (XGBoost) algorithm performs parallel tree boosting, and gained reputation after winning several Kaggle competition problems [30,31].

Since training a model on acquired data can be subjective to patterns and observations that are identified on previously generated data, prediction efficiency may suffer on new data. Bagging and boosting are randomization methods known as ensemble strategies involved to avoid overfitting [30,31]. Alternatively, k-fold cross validation (CV) arises as a necessary process to generalize a model (especially, non-tree algorithms) by separating and testing random partitions (repeated hold-out), and is commonly part of industrial AI approaches [32]. There is no panacea in model selection for a specific problem. Consequently, sophisticated tuning or model ensembles are often required to improve prediction metrics, which is a harsh task in real-life cases. As importantly, the hyperparameter tuning is involved, since hyperparameters can significantly affect predictive ability; proper tuning is necessary since there is no global optimum approach in order to deal with overfitting occasions [26]. For instance, accuracy of ANNs is dependent on the number of repetitions, the network topology (number of layers and neurons), learning rate, dropout rate [17,26,33]. Bagging of decision trees enables the tuning of many hyperparameters, namely size, number of classifiers, number of trees, maximum instances per leaf, and maximum depth [17]. These hyperparameters deviate significantly in case studies of different fields.

Nanoindentation is a technique that can provide experimentally verified input for modeling in order to simulate mechanical performance and failure of composite structural elements [2]. Reduced Elastic modulus (E_r) has been previously involved in design implementations in construction field [34,35]. Additionally, a wide range of construction materials and coatings has been studied through nanoindentation, namely micro- and nano- reinforced composites, metal alloys, coatings, and concrete, since it combines fast and precise characterization [18,19,21,22,24,36–40]. High-resolution mapping in case of CFRPs can be obtained at low indentation depth in order to determine single-phase mechanical properties of CFs, epoxy matrix (often affected by fiber constraint), and interface [6,41,42]. Consequently, the motivation of this study is to use ML on CFRPs nanoindentation raw data to establish novel relationships between structure (reinforcement mechanism) and properties (nanomechanical performance). Neural Networks, classification trees, and SVM were involved in order to evaluate which model has a better fitting ability to recognize the mechanism of reinforcement in the specific problem. Three modification classes were identified to categorize nanoindentation data. The classes are mentioned as pristine, with oxygen functionalities “oxygen_species”, covered with polymer sizing “CF_pmaa”, and modified by the growth of carbon nanotubes (CNTs) “CNTs_CFs”. Since, classification of reinforcement mechanism in CFRPs using AI is a novel task in composites field, a number of techniques were selected to choose an optimum descriptive model based on prediction metrics.

2. Materials, methods and workflow

2.1. Composite manufacturing and carbon fiber functionalization

Carbon fiber reinforced polymer specimens received were characterized through nanoindentation. The specimens tested varied in

order to represent an ontology of surface modification of CFs each, accordingly:

a) CFRPs with unfunctionalized CFs (5 Pristine specimens)
b) CFRPs fabricated using CFs with surface functionalization with oxygen groups, such as Plasma functionalization (3 oxygen_spieces specimens) – the reinforcement mechanism is identified in increment of chemical affinity of CFs surface and epoxy matrix
c) CFRPs reinforced with CFs functionalized with monomer grafting (3 electropolymerized with PMAA specimens) – the reinforcement mechanism is a combination of increased surface roughness, due to the brush-like structure of monomer grafting on CFs, and increment of chemical affinity, which both enhance wettability with epoxy matrix
d) CFRPs with interfacial reinforcement using the direct growth of CNTs on CFs surface (2 growth_CNTs specimens) – the reinforcement mechanism is attributed due to increased CFs rigidity

Synthesis and chemical modification are available in previous works [9–11]. Composites were fabricated with the vacuum infusion method for the impregnation with epoxy resin.

2.2. Grid nanoindentation

Nanoindentation testing was conducted with a Hysitron (Minneapolis, MN, USA) TriboLab® Nanomechanical Test Instrument equipped with a Berkovich diamond tip (average radius 100 nm). Load and displacement are continuously recorded with high resolution of 1 nN and 0.04 nm, respectively. Further information about both instrument and experimental setup have been presented elsewhere [36]. The nanoindentation protocol included a fixed maximum indentation depth at 200 nm in accordance to rule of thumb ($d/10 \ll h_{max} \ll D/10$, d and D stand for the characteristic sizes of the largest heterogeneity) [43], and the pristine specimen was also tested at 400 nm depth for the validation of ML models. Prior to indentation, the area function was calibrated with a standard material of fused silica. Nanoindentation was performed in a clean area environment with 45% humidity and 23 °C ambient temperature with displacement feedback control closed loop. A pattern (Fig. 1) with minimum spacing of 5 μm was used in order to avoid any indentation-to-indentation interaction [21]. Load-unload curves were fitted with Oliver-Pharr model using the elastic response within the region of maximum load of unload curves to extract nanomechanical properties [44].

In order to meet flat surface requirements for nanoindentation, specimens were wet polished using SiC grinding papers. The applied grinding and polishing protocol contained the treatment with consecutive use of 400,1000, 1200, 2000 and 4000 grit papers for a duration of 10 min each by using Struers LaboPol-2 grinding, lapping and polishing machine. The specimens were treated with ultrasonication for 3 min to detach the Al_2O_3 particles that were used in ethanol dispersion during the polishing step.

2.3. R language

R Studio is an open-source software and provides a coherent, flexible system for data analysis. R language was used to implement every algorithm involved in clustering and classification tasks. All computations were performed using 64-bit Windows 10 Home (Intel ® Core™ i5-8250U CPU @ 1.60 GHz, 1801Mhz 4 Cores, 8 Logical Processors and 8.00 GB RAM).

2.4. Statistical metrics

In order to evaluate the prediction efficiency of the trained models, statistical metrics are involved. Accuracy, Precision, Recall, F1 were exported in each case [20,31,45,46], after tuning. These metrics are maximized when the model does not generate false positive or false negative predictions as can be observed below [33]:

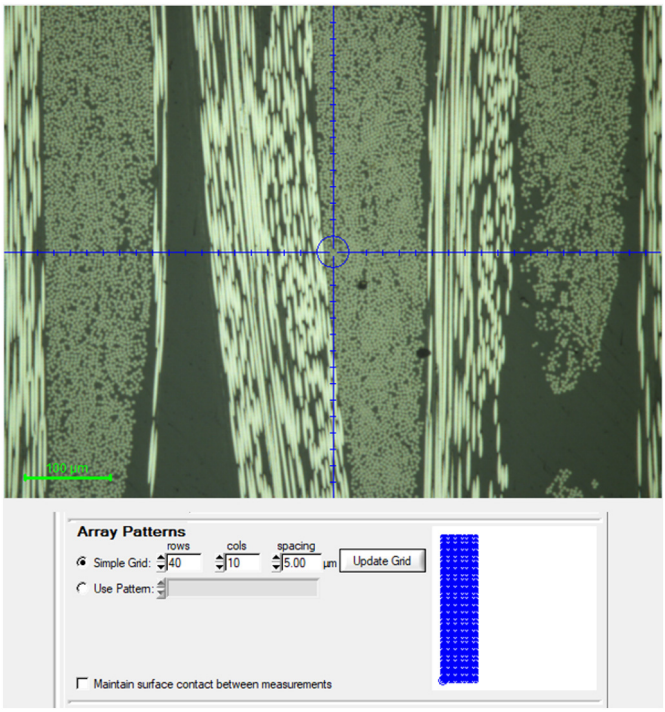

Fig. 1. Nanoindentation grid for CFRPs characterization.

$$Accuracy = \frac{TP + TN}{TP + TN + FP + FN} \quad (1)$$

$$Recall = \frac{TP}{TP + FN} \quad (2)$$

$$Precision = \frac{TP}{TP + FP} \quad (3)$$

$$F1\ Score = 2 \times \frac{Precision \times Recall}{Precision + Recall} \quad (4)$$

True positives (TP) denote the success in identification of the correct reinforcement class (positive sample), true negatives (TN) denote successful classification of negative samples, false positives (FP) stand for the incorrect classifications of negative samples into positive samples, and false negatives (FN) denote the positive samples that were incorrectly predicted as negative samples [33]. Accuracy accounts for overall model accuracy. Recall is the percentage of positive samples which are correctly classified. Precision is the percentage of positive samples out of the sum of positive observations. F1 Score is a metric to evaluate the model ability to classify (best value:1). These metrics are more appropriate metrics than Accuracy [33]. MicroAvgPrecision, MicroAvgRecall, MicroAvgF1 are metrics derived by the sum of the individual true positives, false positives, and false negatives of the system for different sets. Micro-metrics are expected to obtain the same value because there is only one class associated with each instance [46]. MacroAvgPrecision, MacroAvgRecall, MacroAvgF1 are mean values for overall model metrics.

3. Case study: recognition of reinforcement mechanism in CFRPs

3.1. Data preprocessing

Nanoindentation raw data were obtained from several nanoindentation mapping tests (a total of 2461 indentation events and 400 in number for the validation dataset). The column names were set identical with R language for each .txt file generated in order to avoid creation of N/A (not available) values. Numeric cells were prepared for clustering and classification using Standardization (or z-score normalization) in order to avoid bias due to parameters' different scale of magnitude. The correlation matrix was created for all 9 nanoindentation variables to figure and sort out parameters of high correlation, which are connected to models overfitting issue [26,31]. The recorded variables are summarized in Appendix (Table A.1). Variables with very strong correlation exceeding the value of ±0.90 were not included for analysis (Fig. 2) [31,47].

3.2. Preparation of data for Machine Learning

Due to the high similarity of matrix nanomechanical properties in all CFRPs, inclusion of their data in classification models may harm Accuracy, Recall, Precision, and F1 Score due to the generation of many false positive and false negative values. Since the reinforcement is identified in the interfacial and CFs properties and not in the matrix, it was reasonable to remove these data. The number of clusters was selected with pure probabilistic basis [48]. In this direction, k-means algorithm was involved to categorize data into 5 clusters according to elbow rule as presented in Fig. 3. This is further supported by the Humbert index, which is a correlation coefficient of indicator variables connected to intra-cluster distance (indices) such as mean value, standard deviation, etc. It is a graphical method for determining the number of clusters (Fig. 3b), where the observation of a significant peak corresponds to respective increase in the value of the measure. In this case, amongst all indices, 5 indices proposed 4 as the best number of clusters, while 15 proposed 5 as the best number, and only 3 proposed 8. According to the majority rule, the best number of clusters is 5. Then the two clusters with the higher values of hardness were selected, since it is a measure which is a straightforward outcome of nanoindentation testing. Thus, intrinsic properties of interface can be identified. Then data were treated by randomizing the sequence of rows to ensure that there is no chance to introduce bias during model training. A sample of randomized data is available in Appendix (Fig. A.1). Splitting in this case was set to 72% for train (composed from CF_pmaa: 190, growth_CNTs: 176, oxygen_species: 228, pristine: 286), 7% for test (composed from CF_pmaa: 18, growth_CNTs:18, oxygen_species: 27, pristine: 25) datasets. For validation of models, a pristine CFRP was tested at higher indentation depth of 400 nm in order to demonstrate the model functionality even at different (low-) depth nanoindentation. Validation dataset was consisted of 256 nanoindentation events (21% sample of all available data after filtering and sorting out with k-means clustering).

3.3. Artificial neural networks (ANN)

ANN were involved in the effort to establish correlations of nanoindentation data in CFRPs case. The main drive is that ANNs perform as a black box method and can learn very complex patterns of data [26,32,33] as in the case of reinforcement mechanism identification task. A first effort was performed using the Stuttgart Neural Network Simulator (SNNS) algorithm. The main feature is the low-level interface, while it also contains the default high-level interface of ANNs. The train control of this model contained a 10-fold randomized cross validation, repeated for 10 times using the default summary function. The tune length was set to 20 and the optimization metric used in this case was accuracy. In order to improve prediction, MLP ANNs with three layers were chosen. The default parameterization of SNNS algorithm was initially used. The same algorithm was also tuned by introducing weight decay parameter using non- and repeated CV and keeping constant the tune length (20). When training ANNs, it is preferable to use weight decay regularization method [17,49], where after each update, the weights are multiplied by a factor slightly less than 1. This prevents the weights from growing too large, and can be seen as gradient descent on a quadratic regularization term. In this case, decay was tuned using values of *0*, *0.00001*, *0.0001*, *0.001*, *0.01*, *0.1* amongst the three neural network layers. To continue with the pursue of a higher F1 Score in this multiclass classification problem, and thus minimization of false positives and false negatives, an Averaged Neural Network (avNNet) model was used. Again, train control was kept the same, and grid search of optimum hyperparameters contained decay values as mentioned before, and *size* hyperparameter varied between *5*, *10*, and *20*. For each repeat, bagging was enabled by using this model. The confusion matrix of the aforementioned trained and tuned ANNs models is presented in Appendix (Table A.2) and statistic metrics are summarized in Table 1 (full table of metrics is available in Appendix - Table A.3).

In Table 1 it can be observed that decay addition in model parameterization improved overall prediction accuracy. The best neural network performance (MLP with decay) demonstrated a better recognition ability for CFRPs reinforced in the interface using monomer grafting as sizing, and also CNTs growth. This demonstrates that the best tuned neural network is sensitive in the correct detection of the reinforcement mechanism based on increment of CFs surface roughness, based on modifications which decorate the surface of CFs. This is an indication that weight amongst classes is a critical parameter during patterning with neural networks, since avNNet algorithm lead to a 62.5% prediction accuracy, which is comparable to the maximum 63.6% achieved with weight decay introduction. By comparing models

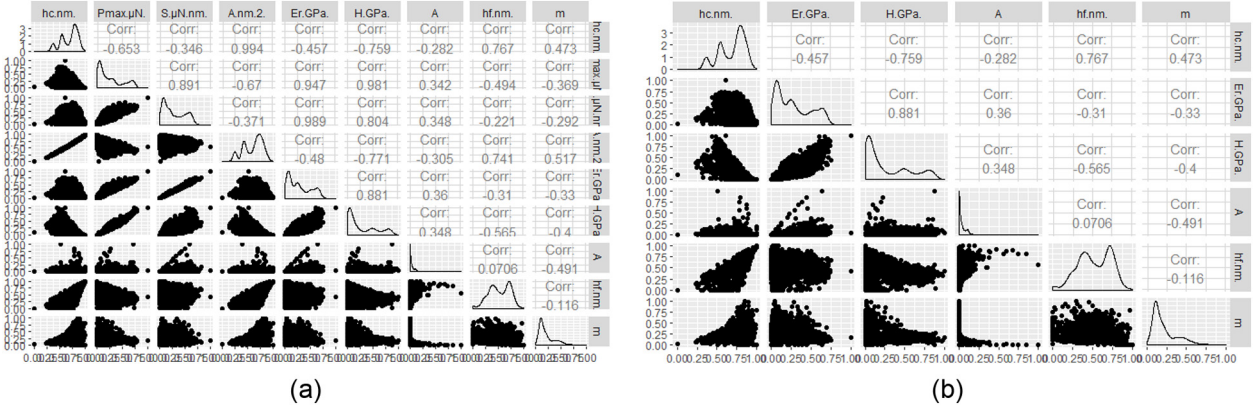

Fig. 2. Correlation matrix of nanoindentation data prior (a) and after (b) sorting out parameters of very strong correlation.

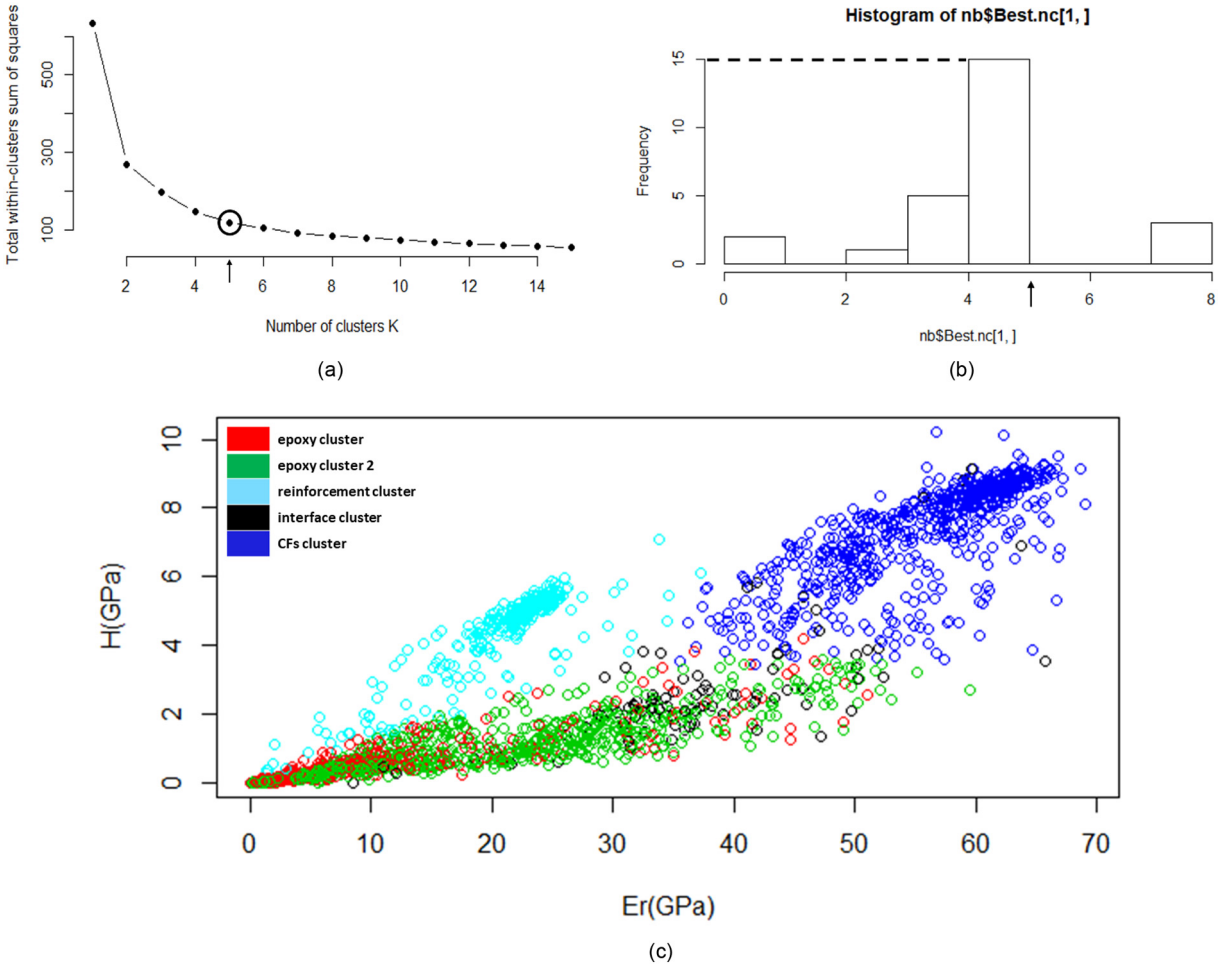

Fig. 3. Determination of optimum number of clusters (noted for a,b) with (a) the elbow method, (b) Humbert criterion, and (c) H vs E_r clusters plot.

micro- and macro- metrics, MLPs with decay demonstrated the higher values of micro-metrics, whereas MLPs with weight decay and non-repeated CV lead to the highest macro-metrics (Table A.3). Moreover, this model was chosen as preferable for reinforcement detection, since two out of the three Precision and Recall metrics exceeded in performance the other models and thus a higher F1 Score was achieved in the prediction of different interfacial reinforcement. It is worth to mention that the number of false positive classifications are also reduced when the reinforcement is performed with PMAA and CNTs deposition (Table A.2), which both differ to oxygen functionalization in both chemistry, dimensionality, and stereochemical structure.

3.4. Classification trees

Initially, Random Forrest (RF) algorithm was employed as the simplest approach to implement classification trees. *mtry* hyperparameter was set as *2* as implied by the empirical rule for the classification problem (the integer square root of number of variables - 6 in total - equal to *2* or *3*, and *ntrees* was set as *70*). An acceptable Precision metric was achieved for the prediction of polymer sizing and CNTs functionalization reinforcement mechanism; however, prediction of pristine and oxygen functionalization classes was below par. Except for pristine class, high Precision lead to low Recall, and the opposite. F1 Score was in all cases

Table 1
Prediction metrics of 4 ANNs algorithms on test data. The best scores are reported in bold.

	SNNS MLP				MLP with decay (default CV) Time elapsed: 114 min			
	CF_pmaa	Growth_CNTs	Oxygen_species	Pristine	CF_pmaa	Growth_CNTs	Oxygen_species	Pristine
Accuracy	0.580				**0.636**			
Precision	0.611	0.556	**0.593**	0.560	**0.778**	**0.667**	0.556	0.600
Recall	0.500	0.625	0.615	0.583	0.560	**0.800**	**0.652**	0.600
F1	0.550	0.588	0.604	0.571	**0.651**	**0.727**	**0.600**	**0.600**
	MLP with decay (repeated CV)				avNNet			
	CF_pmaa	Growth_CNTs	Oxygen_species	Pristine	CF_pmaa	Growth_CNTs	Oxygen_species	Pristine
Accuracy	**0.636**				0.625			
Precision	0.611	0.556	**0.593**	**0.760**	0.722	0.556	**0.593**	0.640
Recall	**0.611**	0.667	0.615	**0.655**	0.542	0.714	0.640	0.640
F1	0.611	0.606	0.604	0.704	0.619	0.625	0.615	0.640

above 50% (0.5 out of 1), but only two classes were predicted with F1 equal or higher 0.6. In order to improve results, tuning of the algorithm was performed with optimization metric "Kappa" in one case, and "Accuracy" in the other case. The control function was coded to perform of 10-fold CV repeated for 10 times. When changing optimization metric to Accuracy, the results did not alter since the hyperparameters that maximized Kappa, also lead to a maximum Accuracy. Also, both tuned models deteriorated significantly the sensitivity in identification of CNTs reinforcement, in favor of enhancing prediction of pristine class, as both Precision and Recall were increased. Another algorithm, rFerns classification tree was trained with 10-fold CV repeated for 10 times, and tune length was set equal to 20 for optimization of accuracy. Still, accuracy did not exceed the performance of the plain RF algorithm; even though F1 Scores were more balanced, leading to a 57.1% score in the worst predicted class. It is interesting to note that statistic metrics are the same for polymer sizing and the pristine specimen for tuned RFs and rFerns models, while prediction of the other classes was improved (Tables A.4, A.5).

Considering the large variety of known classification trees, it was regarded worth to test more models to improve prediction in the present case classification problem. Thus, Ranger algorithm was implemented since additional features can be tuned. Tune length and train control were kept the same as before, but *mtry* parameterized between *1*, *2*, *3*, and *4* to identify the value that lead to best accuracy, while node size was tuned between *1*, *5*, *10*, and *15*. The number of trees was set at *500*, optimum *mtry* parameter was set at 4, and minimum node size was *15*. The same approach was examined by changing the summary function. This time the optimum *mtry* was equal to *3*. In both cases, accuracy was reduced compared to previous models. Prediction favored the identification of polymer sized and pristine CFRPs, but this was not enough to cover the needs of the present study. Rpart algorithm was applied with the 10-fold CV protocol. The algorithm was implemented with tuning *maxdepth* parameter in the range from *2* to *20*, in order to achieve higher accuracy. Rpart did not lead to higher accuracy, but it was possible to exceed the threshold of 0.6 in three out of four cases. In this model, the performance was improved in regards to Recall, and F1 Scores () which were 63.2% for polymer sizing, 66.7% for the case of grown CNTs, 56.5% in case of oxygen functionalization, and 64.2% for pristine class; ideally, F1 Score should be further increased.

As a following step, bagging of classification trees was applied by only setting hyperparameter *nbag* to *25* and to 5000 for differentiation. Another tree bagging approach did not include setting *nbag* parameter, however it was possible to perform 10-fold CV repeated for 10 times. Compared to Rpart, prediction was not improved, and got even worse for *oxygen_species* class with F1 Score below 0.5 when *nbag* value was low Even at higher *nbag* the prediction metrics were not sufficiently high. Crossvalidation on trees model with bagging resulted below par prediction in *growth_CNTs* class.

The famous *C5.0* algorithm was involved to deal with the weaknesses in identification of reinforcement mechanism that were encountered with the applied classification trees models, since it is proved to function well with real-life problems at industrial level [32]. Classification was performed by boosting the tree algorithm using *10* trials. By increasing the number of trials to *25*, results are slightly altered. No significant changes occurred after performing *75* trials. In case of *25* trials, the model lead to a higher F1 Score than 0.60 in all classes except for *oxygen_species*. Boosting was performed by using an additional feature of a cost matrix in order to introduce a penalty for false negative values that appear for the *oxygen_species* class. Also, crossvalidation (10-fold, 10 repeats) was performed in a grid of hyperparameters. In detail, classification was performed using a "*tree*" or classification "*rules*", and *winnow* was set either *TRUE* or *FALSE*. Boosting trials varied from *10* to *90* with a step of *10*. Neither these efforts were efficient to resolve the weakness in F1 Score value of *oxygen_species* without sacrificing the prediction of the rest classes. AdaBoost, short for Adaptive Boosting, is a meta-algorithm. The output of the other learning algorithms ('weak learners') is combined into a weighted sum that represents the final output of the boosted classifier. Adaboost was used without any prior tuning, and the majority of prediction metrics did not exceed the performance of Rpart algorithm, but for *oxygen_species* class F1 Score, which was improved by 2.3% (58.8% in total) (Table 2).

Furthermore, Stochastic Gradient Boosting algorithm was used for classification. Multiple hyperparameters were tuned using a grid search. Interaction depth was selected equal to *1*, *5*, and *9*, number of trees "*n.trees*" was tuned from *50* to *1500* with a step of *50*. *Shrinkage* was set constant at *0.1* and minimum number of nodes "*n.minobsinnode*" was set at *20*. This resulted in good prediction of pristine (highest Precision amongst all tree models) and polymer functionalized classes (higher Recall amongst all tree models, macro- and micro- metrics are available in Table A.5). However, the other two reinforcement mechanisms could not be sufficiently predicted, since F1 Score slightly exceeded 0.50. Also, xtreme gradient boosting trees were used. Hyperparameters grid tuning values varied between *0.05*, *0.3*, *0.075* for *eta*, *50*, *75*, *100* for *nrounds*, *4*, *5*, *6*, *7* for *max_depth*, *2.0* and *2.25* for *min_child_weight*. *colsample_bytree* was set in between *0.3*, *0.4*, *0.5*, and subsample value was set to *1*. Train control was performed using a 10-fold repeated crossvalidation for 10 times. This was not very effective, since overall accuracy was 55.7%. In order to improve results, in another trial *eta* value was set at *0.01*, *max_depth* to *5*, *gamma* hyperparameter was involved to deal with values that deteriorate model accuracy and was set to *3*. Additionally, *subsample* was set to *0.75*, *colsample_bytree* was set to *1*, and *mlogloss* was used as an evaluation metric. The model was established after performing a total of 10,000 training repetitions. For comparison, a decrement in *eta* value at *0.001*, and increment in *max_depth* to *15* for a total of 100,000 rounds was performed to train the model at higher accuracy. In both occasions the highest accuracy achieved was 63.6%, with the main difference the highest computational cost of performing 90,000 additional training repetitions. However, the minimum F1 Score was 60%, which was influenced by the reduction of false negatives (full Tables are available in the Appendix - Table A.4), while the other three classes were predicted with a score of almost 65% and thus this model was selected for deployment in the validation dataset. Also, micro- and macro- metrics were the highest achieved within classification trees (full Tables are available in the Appendix - Table A.5).

The optimization of classification trees were realized only after using boosted trees, which function in the background as a voting system in to make one classification. This approach lead to higher accuracy by optimizing the Precision metric in oxygen_spiecies class, compared to the rest of classification trees involved. This fact indicates that models ability in correct prediction of oxygen_spiecies was increased; however, this approach demonstrated a balanced framework for recognition of the engineering procedure, which falls behind the interface reinforcement.

3.5. Support vector machines – SVM

Radial kernel function was chosen initially to describe the nanoindentation data. The SVM model was tuned using a grid for determination of optimum *cost* (*1*, *10*, *50*, *100*, *400*, *1000*, *4000*) and *gamma* (*0.01*, *0.1*, *0.5*, *2*, *4*) values, which were *400* and *0.1*, respectively. In addition, a polynomial kernel was used in order to investigate if prediction metric could be further improved. Tuning process was more complex, since 4 hyperparameters were investigated. These are *degree* (*3*, *4*, *5*), *coef0* (*0.1*, *0.5*, *1*, *4*, *8*, *12*), *gamma* (*0.1*, *1*, *4*), and *cost* (*1*, *10*, *50*, *100*, *400*, *1000*, *4000*). Consequently, parameters with highest accuracy were identified ($degree = 5, gamma = 0.1, coef0 = 12, cost = 1$). Gaussian kernel function was used with manual tuning, since automation of tuning process is challenging. *Sigma* hyperparameter was set as 5 and *cost* varied amongst *1*, *40*, *100*, *400*, and *1000*. CV was repeated 10 times and *sigma* parameter was set at 3. Increment in *sigma* value to *4* did not improve predictions (Table 3).

Table 2
Prediction metrics of selected classification tree algorithms on test data. Full Tables are available in the Appendix A. The best scores are reported in bold.

	RF				RF tuning (Kappa)			
	CF_pmaa	Growth_CNTs	Oxygen_species	Pristine	CF_pmaa	Growth_CNTs	Oxygen_species	Pristine
Accuracy	0.625				0.602			
Precision	**0.833**	**0.778**	0.444	0.556	0.778	0.444	**0.556**	0.640
Recall	0.577	0.519	0.667	0.577	0.519	**0.667**	0.577	0.696
F1	0.682	0.622	0.533	0.566	0.622	0.533	0.566	0.667
	RF tuning (accuracy)				rFerns (tuned)			
	CF_pmaa	Growth_CNTs	Oxygen_species	Pristine	CF_pmaa	Growth_CNTs	Oxygen_species	Pristine
Accuracy	0.602				0.614			
Precision	0.778	0.444	**0.556**	0.640	0.778	0.667	0.519	0.560
Recall	0.519	**0.667**	0.577	0.696	0.519	0.500	0.700	**0.824**
F1	0.622	0.533	0.566	0.667	0.622	0.571	0.596	0.667
	Trees with bagging (nbag = 5000)				C5.0 boosting (25 trials)			
	CF_pmaa	Growth_CNTs	Oxygen_species	Pristine	CF_pmaa	Growth_CNTs	Oxygen_species	Pristine
Accuracy	0.614				0.614			
Precision	**0.833**	0.556	0.481	0.640	0.778	0.667	0.444	0.640
Recall	0.577	0.588	0.650	0.640	0.560	0.632	**0.750**	0.571
F1	0.682	0.571	0.553	0.640	0.651	0.649	0.558	0.604
	XGBoost (with gamma, 10,000 rounds)				XGBoost (with gamma, 100,000 rounds) Elapsed time: 84 min			
	CF_pmaa	Growth_CNTs	Oxygen_species	Pristine	CF_pmaa	Growth_CNTs	Oxygen_species	Pristine
Accuracy	**0.636**				**0.636**			
Precision	0.722	0.667	**0.556**	0.640	0.722	0.667	**0.556**	0.640
Recall	0.591	0.632	0.682	0.640	0.591	0.632	0.652	0.667
F1	0.650	0.649	0.612	0.640	**0.650**	**0.649**	**0.600**	**0.653**

The radial-shaped kernel provided the optimum predictions with accuracy of 67% amongst other kernels. Radial kernel established a higher accuracy by patterning the normality of standard reinforcement. Especially, if the recognition of the reinforcement mechanism was to answer whether the CFs have been modified in the surface, the task would be tackled with great success. Still, the identification of correct chemistry to mechanical interlocking effect is high as demonstrated by the F1-scores. In opposite, polynomial kernel was biased to predict efficiently with 74.4% polymer sizing reinforcement and with 73.5% pristine CFRPs, but Precision was not sufficient for the other two classes compared to radial kernel as demonstrated in (more details in Tables A.6 and A.7). By using Gaussian kernel, the Recall is reduced by almost 10% for prediction of *oxygen_species* and *Pristine* classes, while it is significantly enhanced in case of *growth_CNTs*, but reduction in Precision negatively affected F1 Score. Thus, Radial SVM model was adopted for predictions in validation dataset, since the F1 Score was almost 65% in all occasions of reinforcement, and 72% for the *pristine* class.

3.6. Summary of the results

The implementation of ML algorithms demonstrated that it is possible to recognize the surface modification of CFs by nanoindentation testing. The properties of the reinforced composites are dependent in the nature of functionalization technique applied on CFs, and mechanical interlocking can be matched to the engineering of CFs. The three different modification treatments studied differed in surface chemistry, i.e. plasma modification increased the chemical affinity of epoxy matrix and CFs, carbon nanomaterials functionalization increased rigidity of CFs surface, while PMAA electropolymerization can provide both kinds of reinforcement; by enhancing chemical affinity and surface roughness in a brush-like decoration of CFs. The classification of the true class of reinforcement and the correct dismission of an indentation point that does not belong to the real reinforcement is a great challenge, since it is not straightforward. This was not possible by the original nanoindentation data, and this is the reason why clustering was involved in data

Table 3
Prediction metrics of 4 SVM algorithms on test data. The best scores are reported in bold.

	Radial kernel Elapsed time: 2.3 min				Polynomial kernel			
	CF_pmaa	Growth_CNTs	Oxygen_species	Pristine	CF_pmaa	Growth_CNTs	Oxygen_species	Pristine
Accuracy	**0.670**				0.659			
Precision	0.722	**0.667**	0.593	0.720	**0.889**	0.556	0.519	**0.720**
Recall	0.591	0.632	0.727	0.720	**0.640**	0.556	0.667	0.750
F1	**0.650**	**0.649**	**0.653**	**0.720**	0.744	0.556	0.583	0.735
	Gaussian kernel (Sigma = 3)				Gaussian kernel (Sigma = 4)			
	CF_pmaa	Growth_CNTs	Oxygen_species	Pristine	CF_pmaa	Growth_CNTs	Oxygen_species	Pristine
Accuracy	0.648				0.648			
Precision	0.722	0.500	**0.630**	0.720	0.722	0.500	0.593	**0.760**
Recall	0.591	**0.818**	0.654	0.621	0.591	**0.750**	0.640	0.655
F1	0.650	0.621	0.642	0.667	0.650	0.600	0.615	0.704

preprocessing. Epoxy matrix properties do not depend on interfacial reinforcement and were identified by k-means clustering. This strategy enabled the recognition of the reinforcement mechanism. The actual reinforcement is obtained in interface and CFs properties and by using ML it is possible to use nanoindentation data not only to perform mapping of nanomechanical properties, but also reveal the chemistry of CFs and the mechanism that is realized behind mechanical reinforcement. The best tuned ANN algorithm facilitated the detection of functionalizations that enhance mechanical interlocking through the increased surface roughness of CFs surface as a mechanism for enhanced wettability with the epoxy matrix during impregnation. In case of boosted classification trees, a better balance between correct classification of reinforcement classes, as demonstrated by the F1-score. Especially, XGBoost (boosted) trees demonstrated better classification performance compared to other classification trees, due to the enhanced functionality of the voting system to correlate nanomechanical properties to the chemical footprint of the modified CFs surface. The best performance according to F1-score was achieved with SVM classification using a radial kernel, which patterned the normality of the standard CFRPs, in order to correctly identify the intrinsic difference of each modification and predict accordingly the reinforcement mechanism, using nanomechanical properties as input. Also, SVM required the least time of 2.3 min to deal with the recognition of reinforcement mechanism.

The priority when using ML in material science tasks is identified in achieving the best accuracy possible. Transparency and interpretability of the used models is not always relevant; accuracy of prediction is more important than the understanding of the algorithms functionality in the multidimensional field to find the required descriptors and establish structure-property relations that are not foreseen with conventional analysis [50]. This is originated by the strength of an accurate model that can have in decision making, design, and optimization through the prediction of the properties of an application-oriented composite fabrication. State-of-the-art research commonly deals with challenges in decision-making to satisfy the needs for composites design that combine multifunctionality and smart properties with performance. As a result, it was necessary to test multiple ML algorithms amongst the plethora of them available, and find the candidates that could predict the mechanism of reinforcement. Accuracy is an important prediction metric; however, models can achieve similar accuracy, and thus choice of the appropriate algorithms fall within precision, recall, and their combination in the F1-score metric. Maximization of F1-score indicates the minimization of misclassification error, which is essential when the number of classes is high, as presented in the present case.

As demonstrated in Fig. 4, accuracy of radial SVM kernel exceeds the performance of ANN MLP and XGBoost algorithm by 3.4%, which may not be considered as an actual improvement in functionality. Further insights are derived by the prediction metrics. Boosted classification trees (XGBoost) were outperformed by the other two selected models, as demonstrated by the F1-score (combination of Precision and Recall). ANN MLP algorithm demonstrated higher Precision in the PMAA electropolymerized class, but Recall was deteriorated due to the increase in false negative predictions (Table A.2). Thus, F1 score is equal for all the models involved. Also, ANN MLP provided the highest Recall in growth_CNTs class, which lead in 7.8% higher prediction efficiency in this class; however, the F1-score for the prediction of oxygen_species and Pristine classes was the lowest (60%). On the other hand, radial SVM kernel combined higher efficiency in prediction of more classes, while a minimum of 65% F1-score was achieved, which was a challenging task in the identification of reinforcement mechanism. A balance in the prediction of each class is expected to improve transferability of the trained models in new data produced by nanoindentation testing using the same protocol.

Another motivation to choose the best performing algorithm from each classification "family" of models is the different functionality during the patterning of data. This severely affects the transfer learning to

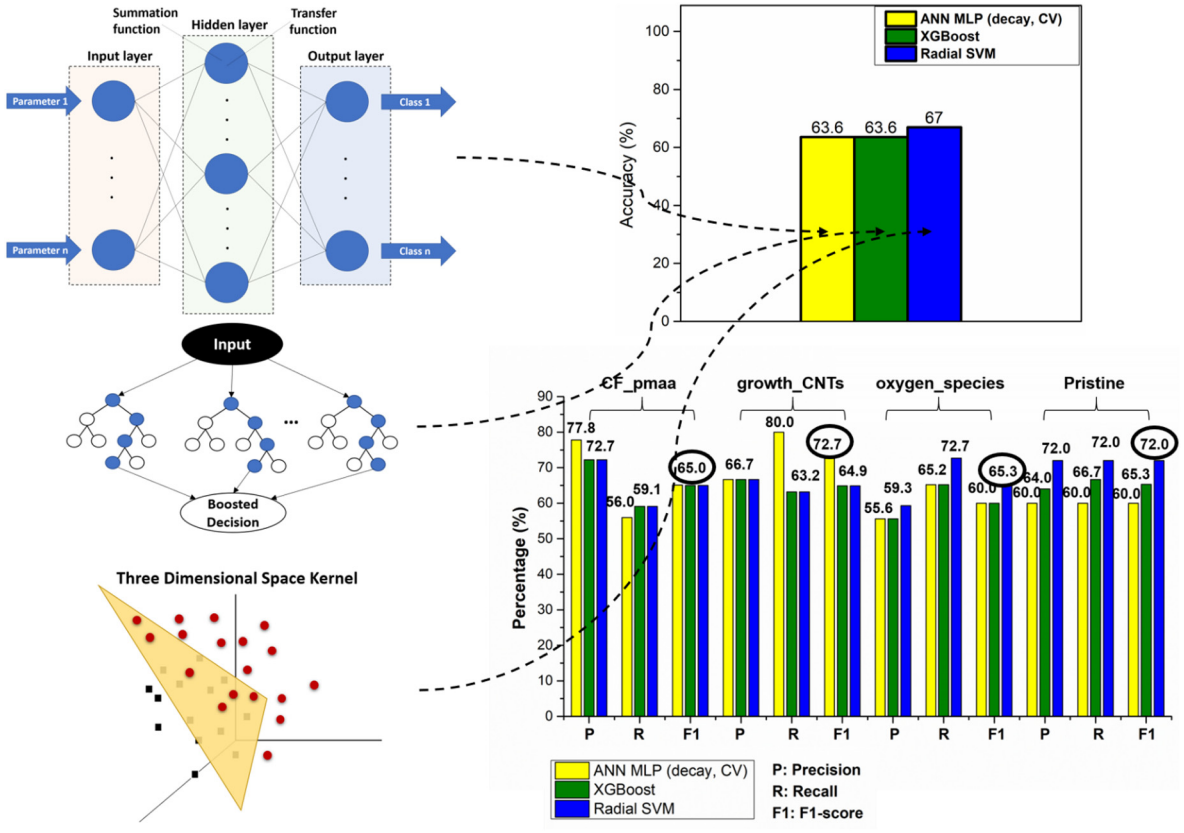

Fig. 4. Comparison of average predictive ability of the best performing algorithms as presented in 3.3, 3.4, and 3.5. A schematic of classification procedure is presented in the left side.

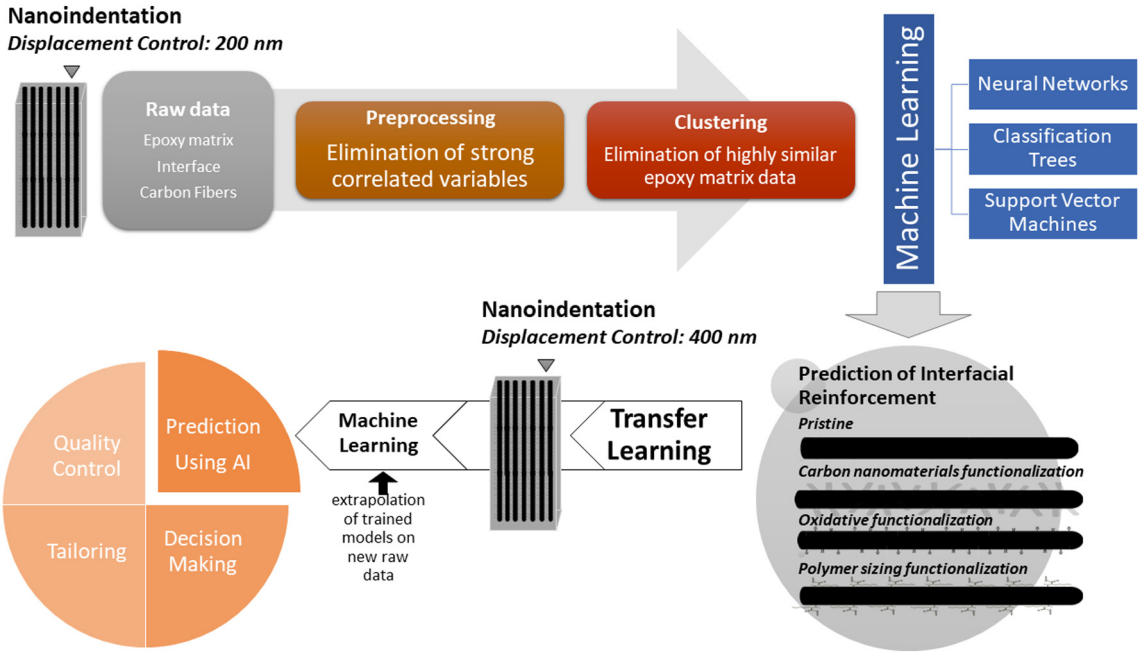

Fig. 5. Workflow of Identification of Reinforcement Mechanism in CFRPs using AI.

new data, i.e. CFRPs tested under different nanoindentation depth. As there is no general rule for choosing a specific algorithm that "performs well" in every problem, the identification of the three more suitable algorithms, with different functionality each, is an achievement for the impact of the developed models for this ML task, due to the ability of the different descriptors in handling new data. This also provides flexibility when the models are deployed for actual evaluation of produced data.

3.7. General discussion of the results

In the preparational steps of ML models training, nanoindentation data variables were associated by two using a correlation matrix. Parameters with very strong correlation were sorted out in order to prevent overfitting. K-means clustering was involved in all occasions for filtering epoxy matrix indentation data before splitting and testing the trained models with the testing and the validation datasets. Since the data were prepared, three categories of ML algorithms were used in this study, artificial neural networks, classification trees, and SVM to investigate their suitability for the specific problem. Identification of interface reinforcement as implemented using AI is summarized in Fig. 5. Tuning parameterization often lead to improvement of either Precision or Recall, but not both, unless the overall accuracy was improved [25]. Radial SVM kernel was a better selection to predict the *oxygen_species* reinforcement, while also exceeding in prediction performance the pristine class compared to *XGBoost* model. Also, radial SVM model proved memory efficient and the fastest to train and tune, as expected [27], with elapsed time of 2.3 min. For

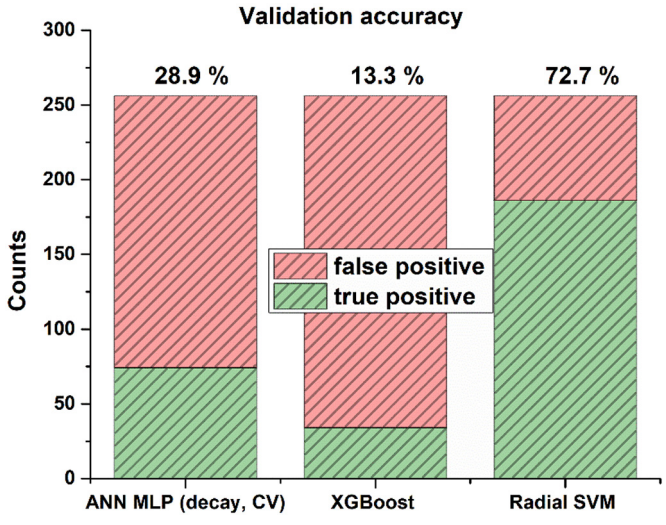

Fig. 6. Prediction performance on validation dataset using the optimum trained ML models.

Table A.8
Confusion matrix of testing the validation dataset on optimum models based on predictions of the test dataset.

	CF_pmaa	Growth_CNTs	Oxygen_species	Pristine
ANN MLP (decay, CV)				
VALIDATION pristine 400 nm				
Elapsed time for training and tuning: 114 min				
CF_pmaa	0	0	0	45
Growth_CNTs	0	0	0	4
Oxygen_species	0	0	0	**133**
Pristine	0	0	0	74
Validation accuracy	0.289			
XGBoost				
VALIDATION pristine 400 nm				
Elapsed time for training and tuning: 84 min				
CF_pmaa	0	0	0	67
Growth_CNTs	0	0	0	1
Oxygen_species	0	0	0	**154**
Pristine	0	0	0	34
Validation Accuracy	0.133			
Radial SVM				
VALIDATION pristine 400 nm				
Elapsed time for training and tuning: 2.3 min				
CF_pmaa	0	0	0	33
Growth_CNTs	0	0	0	36
Oxygen_species	0	0	0	1
Pristine	0	0	0	**186**
Validation accuracy	**0.727**			

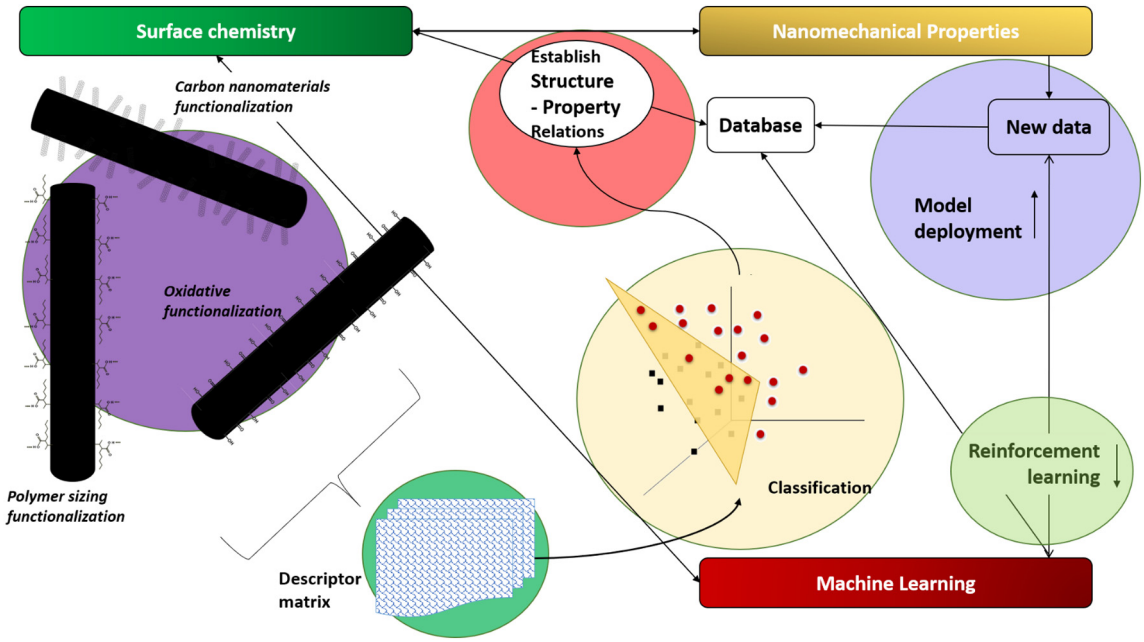

Fig. 7. Summary of problem-solving procedure of CFRPs reinforcement characterization with Machine Learning.

comparison, the best tuned ANN and XGBoost models required 114 and 84 min, respectively.

A very common example reported in regard to AI ethics, is a real-world problem for the prediction of mortality within 5 years by using healthcare generated data. In that case a neural network was used with 69% accuracy rate in this binary classification problem, and the need of enhanced accessibility of data was highlighted in order to improve predictions [26]. In the present study, 63.6% accuracy was achieved by ANN and XGBoost models, whereas 67% accuracy was achieved by the radial SVM model for the four-class classification problem. The requirement for accurate prediction of four classes increases the difficulty level of classification and highlights the present achievement; minimum average predictive efficiency of 65% was realized for each class. This proceeding can be further supported considering the random guess probabilities in a binary- and in a four- class classification task; in the first occasion random guess has 50% for successful classification, while four-class classification has 25% chance for correct random prediction. Consequently, in the present study for classification of CFRPs reinforcement, performance exceeded 40% the performance of a random guess, which is a challenge in real-world ML tasks.

In another real-world problem of traffic prediction, a deep neural network was used with three hidden layers [33]. In this case overall

	Class	hc(nm)	Er(GPa)	H(GPa)	A	hf(nm)	m
1	oxygen_species	0.04928655	0.90938753	1.45846821	1.214502437	0.4889699499	-0.52673324
2	oxygen_species	1.43936517	-0.46703856	-1.43578388	-1.092969238	0.9383679641	0.97559143
3	oxygen_species	0.60813622	0.84788928	0.67472344	-0.803120690	0.0915848508	0.60826275
4	oxygen_species	0.69846085	0.43315052	0.13525872	0.810703447	1.1091362809	-0.44127419
5	oxygen_species	0.30086182	0.85978012	1.07637777	0.939625140	0.6722861821	-0.43126533
6	oxygen_species	0.51482353	0.29743818	0.14445968	-1.288657489	-1.6914822407	2.36885378
7	oxygen_species	0.90981947	0.32895825	-0.25172333	-0.803400967	0.5696872921	0.54472243
8	oxygen_species	0.36562645	0.75644148	0.85467734	1.341666380	0.8711139398	-0.55700384
9	oxygen_species	0.26467646	0.56174939	0.72164655	-1.236892290	-1.4448826282	1.71326365
10	oxygen_species	0.48451933	0.19400905	0.04487268	-0.010712381	0.6455839410	-0.18936423
11	oxygen_species	0.36371932	0.72920941	0.80433382	1.232528263	0.8569161519	-0.53303847
12	oxygen_species	1.29656246	1.22669439	0.28327203	0.809710984	1.6114088678	-0.19416990
13	oxygen_species	0.81121715	0.90933658	0.52100496	1.495061901	1.3199860203	-0.51415428
14	oxygen_species	0.83755087	1.12394630	0.69549270	-0.944608293	0.1495826612	0.91701815
15	oxygen_species	0.28000903	1.05868829	1.31232771	-0.486985277	-0.0105884205	0.28400011
16	oxygen_species	0.31412641	1.00059567	1.25152368	0.844702294	0.6254103067	-0.37302267
17	oxygen_species	0.67535302	0.92389360	0.68895694	0.135089400	0.7803795896	-0.07084013
18	oxygen_species	0.81690247	0.86017259	0.47201701	0.636867453	1.1094731472	-0.27170609
19	oxygen_species	0.43849667	1.10546461	1.19510125	-0.500959685	0.1322648268	0.32328773

Fig. A.1. Sample of the refined dataset.

accuracy was almost 71%. The averaged macro- metrics of this model were 0.686 in case of Precision compared to the best radial SVM model of the present study, which reached 0.675 in this macro-metric (Table A.7). Recall on average was equal to 0.710 for the traffic problem, while in the case of reinforcement mechanism prediction it was 0.667. F1 Score was equal to 0.700 for the traffic classification, compared to 0.668 in the present case. In a lithology eight-class real-world classification problem, RF, AdaBoost, and XGBoost were involved to identify the best candidate [31]. In the first case, Precision varied between 0.50 (lower metric) and 0.84 (higher metric), Recall from 0.69 to 1.00, and F1 Score from 0.59 to 0.84. In case of AdaBoost weaknesses were identified, since the variance for Precision was from 0.00 to 0.79, Recall from 0.00 to 0.86, and F1 Score from 0.00 to 0.83. Finally, XGBoost algorithm outperformed all other models in regard to Precision from 0.70 to 0.92, Recall from 0.74 to 1.00, and F1 Score from 0.74 to 0.96. However, no validation dataset was tested in this case to support deployment of the trained models.

3.8. Transfer learning potential: from 200 nm to 400 nm depth

In order to investigate universality of the trained models, a validation dataset was generated by mapping nanomechanical properties of a pristine CFRP at higher indentation depth of 400 nm. Considering the fact that there is currently no standardized method to perform nanomechanical mapping of CFRPs, it is purposeful to propose a model with prediction efficiency in different indentation depth. This test with the validation dataset at 400 nm constant indentation depth demonstrates the transfer learning potential in the present study. The importance of transfer learning is often demonstrated in training of ML models that are used to perform extrapolation and step beyond training data, in order to predict an unknown situation/behavior [17,32,51].

In case of both ANN and XGBoost models accuracy was unsatisfactory in the validation dataset with obtained accuracy values of 28.9%, and 13.3% (Fig. 6, Table A.8), respectively. This can be attributed to overfitting issue that is often confronted when using decision trees, and also in lack in accessible data in case of ANNs [27]. Unsurprisingly, in case of Radial SVM kernel, prediction accuracy of validation dataset was 72.7% and exceeded the overall model accuracy by 5.7%. This result may be attributed to the reported suitability of SVM models in prediction of small datasets [26].

4. Conclusions

The main conclusions drawn from this work (presented as summary of problem-solving procedure of CFRPs reinforcement characterization with Machine Learning, Fig. 7) are summarized below:

1. k-means clustering was used to preprocess data by filtering out the epoxy matrix, due to the algorithm's efficiency to deconvolute the spatial information of the phase level properties.
2. Weight decay of ANNs was proved as the most efficient neural network to achieve higher prediction accuracy, while XGBoost algorithm outperformed other classification trees and reached the optimum results after 100,000 rounds of training. SVM radial kernel classification was identified as the most suitable model to describe the reinforcement mechanism of CFRPs fabricated with surface treated CFs.
3. The intrinsic changes of CFRPs interface were proven to be effectively patterned through ML models, with the best fit being performed by using SVM with a radial kernel. Model accuracy reached 67% with a lower F1 Score by class of 65% and a highest of 72%. Macro- averaged metrics were compared to real-world problems (either binary or multiclass) and these values in case of Precision, Recall, and F1 Score (0.675, 0.667, 0.668) were slightly below those values.
4. Computational time of radial SVM kernel complies with modern time-efficiency requirements. Classification was performed within 2.3 min using a standard computer.
5. Validation of nanoindentation models was performed using a mapping indentation protocol in different indentation depth with displacement control in order to investigate the transfer learning potential. The performance for deployment to a validation dataset lead to higher accuracy achievement for SVM radial kernel model, which reached the value of 72.7%.

The need for more data is expected to resolve the overfitting of trained models as evidenced in case of classification trees and artificial neural networks, which did not perform well for the validation dataset. Artificial Intelligence dealt with interface reinforcement problem efficiently, and can be proficiently involved in materials design; structure was correlated to nanomechanical properties in order to describe the effect of different chemical structure of the surface to the composite mechanical interlocking mechanism (Fig. 7). Thus, it can provide feedback in a process by the development of AI applications for real-time quality control. Finally, it is expected to enhance decision-making for product manufacturing and provide the ability to approach composites manufacturing through reverse engineering approaches with involving the developed models in relevant code modules. In this direction, the importance of AI combination with innovation in testing, such as high-speed nanoindentation testing (also coupled with other techniques), is expected to accelerate insights in materials design.

CRediT authorship contribution statement

Georgios Konstantopoulos: Conceptualization, Methodology, Software, Validation, Formal analysis, Investigation, Data curation, Writing - original draft, Writing - review & editing, Visualization, Supervision.**Elias P. Koumoulos:**Conceptualization, Methodology, Validation, Formal analysis, Investigation, Data curation, Resources, Writing - original draft, Writing - review & editing, Visualization, Supervision, Funding acquisition, Project administration.**Costas A. Charitidis:**Resources, Writing - original draft, Writing - review & editing, Visualization, Supervision, Funding acquisition, Project administration.

Declaration of competing interest

The authors declare that they have no known competing financial interests or personal relationships that could have appeared to influence the work reported in this paper.

Acknowledgements

This research was partially funded by the EU H2020 Project “Modified Cost Effective Fibre Based Structures With Improved Multi-Functionality And Performance” (MODCOMP) under Grant Agreement no. 685844 and partially funded by the EU H2020 Project “Smart By Design And Intelligent By Architecture For Turbine Blade Fan And Structural Components Systems” (SMARTFAN) under Grant Agreement no. 760779.

Appendix A

Table A.1
Parameters variance before and after normalization.

Raw data	H (GPa)	A	hc (nm)	hf (nm)	Pmax (μN)	M	S (μN/nm)	Er (GPa)	A (nm^2)
Min.	2.37E−03	0.00E+00	7.02E+01	0.00E+00	1.46E+00	1.00E+00	2.59E−02	3.31E−02	1.68E+05
1st Qu.	4.34E−01	7.80E−02	1.40E+02	7.10E+01	2.67E+02	1.41E+00	6.67E+00	7.57E+00	4.44E+05
Median	1.62E+00	8.47E−01	1.65E+02	1.00E+02	9.56E+02	1.60E+00	1.59E+01	2.27E+01	5.82E+05
Mean	3.04E+00	1.73E+00	1.57E+02	1.03E+02	1.39E+03	1.81E+00	2.15E+01	2.69E+01	5.49E+05
3rd Qu.	5.34E+00	2.54E+00	1.74E+02	1.40E+02	2.36E+03	1.99E+00	3.69E+01	4.60E+01	6.47E+05
Max.	1.02E+01	4.35E+01	1.98E+02	1.98E+02	4.13E+03	5.00E+00	5.94E+01	6.91E+01	8.14E+05

z-Normalized data	H (GPa)	A	hc (nm)	hf (nm)		M		Er (GPa)	
Min.	−3.13E+00	−1.32E+00	−4.95E+00	−3.10E+00	(Removed)	−1.69E+00	(Removed)	−2.41E+00	(Removed)
1st Qu.	−7.17E−01	−8.60E−01	−1.13E+00	−7.13E−01		−5.43E−01		−1.12E+00	
Median	−2.52E−02	−2.26E−01	3.03E−01	8.90E−02		−2.72E−01		3.45E−01	
Mean	0.00E+00	0.00E+00	0.00E+00	0.00E+00		0.00E+00		0.00E+00	
3rd Qu.	9.46E−01	9.16E−01	5.56E−01	6.88E−01		4.34E−01		8.86E−01	
Max.	2.02E+00	3.57E+00	2.70E+00	2.84E+00		5.19E+00		1.44E+00	

hc (nm) is the contact depth.
Pmax (μN) is the peak load during a single nanoindentation event.
S (μN/nm) is a continuous variable and represents the stiffness of a material.
A (nm^2) is the contact area.
Er (GPa) is the reduced elastic modulus after fitting the Oliver-Pharr model.
H (GPa) is the hardness after fitting the Oliver-Pharr model.
A, hf (nm), m are the power law coefficients.

Table A.2
Confusion Matrix of test data by the implementation of 4 ANNs algorithms.

	CF_pmaa	Growth_CNTs	Oxygen_species	Pristine
SNNS MLP algorithm				
CF_pmaa	11	2	2	7
Growth_CNTs	1	10	4	1
Oxygen_species	2	5	**16**	3
Pristine	4	1	5	14
MLP with decay (default CV)				
CF_pmaa	**14**	3	2	6
Growth_CNTs	0	**12**	3	0
Oxygen_species	1	3	15	4
Pristine	3	0	7	15
MLP with decay (repeated CV)				
CF_pmaa	11	3	2	2
Growth_CNTs	1	10	4	0
Oxygen_species	1	5	**16**	4
Pristine	5	0	5	**19**
avNNet				
CF_pmaa	13	3	2	6
Growth_CNTs	0	10	3	1
Oxygen_species	2	5	**16**	2
Pristine	3	0	6	16

Table A.3
Prediction metrics of 4 ANNs algorithms on test data.

	SNNS MLP				MLP with decay (default CV) Time elapsed: 114 min			
	CF_pmaa	Growth_CNTs	Oxygen_species	Pristine	CF_ pmaa	Growth_CNTs	Oxygen_species	Pristine
Accuracy	0.580				**0.636**			
Precision	0.611	0.556	**0.593**	0.560	**0.778**	**0.667**	0.556	0.600
Recall	0.500	0.625	0.615	0.583	0.560	**0.800**	**0.652**	0.600
F1	0.550	0.588	0.604	0.571	**0.651**	**0.727**	**0.600**	**0.600**
MacroAvgPrecision	0.580				0.650			
MacroAvgRecall	0.581				0.653			
MacroAvgF1	0.578				0.645			
MicroAvgPrecision	0.580				0.636			

Table A.3 (*continued*)

	SNNS MLP				MLP with decay (default CV) Time elapsed: 114 min			
	CF_pmaa	Growth_CNTs	Oxygen_species	Pristine	CF_ pmaa	Growth_CNTs	Oxygen_species	Pristine
MicroAvgRecall	0.580				0.636			
MicroAvgF1	0.580				0.636			
	MLP with decay (repeated CV)				avNNet			
	CF_ pmaa	Growth_CNTs	Oxygen_species	Pristine	CF_pmaa	Growth_CNTs	Oxygen_species	Pristine
Accuracy	**0.636**				0.625			
Precision	0.611	0.556	**0.593**	**0.760**	0.722	0.556	**0.593**	0.640
Recall	**0.611**	0.667	0.615	**0.655**	0.542	0.714	0.640	0.640
F1	0.611	0.606	0.604	0.704	0.619	0.625	0.615	0.640
MacroAvgPrecision	0.630				0.628			
MacroAvgRecall	0.637				0.634			
MacroAvgF1	0.631				0.625			
MicroAvgPrecision	0.636				0.625			
MicroAvgRecall	0.636				0.625			
MicroAvgF1	0.636				0.625			

Table A.4
Confusion Matrix of test data by the implementation of classification tree algorithms.

	CF_pmaa	Growth_CNTs	Oxygen_species	Pristine
RF				
CF_pmaa	**15**	3	3	5
Growth_CNTs	0	10	5	0
Oxygen_species	2	5	13	3
Pristine	1	0	6	17
RF tuning (Kappa)				
CF_pmaa	14	4	3	6
Growth_CNTs	0	8	4	0
Oxygen_species	2	6	**15**	3
Pristine	2	0	5	16
RF tuning (accuracy)				
CF_pmaa	14	4	3	6
Growth_CNTs	0	8	4	0
Oxygen_species	2	6	**15**	3
Pristine	2	0	5	16
rFerns (tuned)				
CF_pmaa	14	4	2	7
Growth_CNTs	1	12	9	2
Oxygen_species	2	2	14	2
Pristine	1	0	2	14
Ranger tuned (mtry = 4)				
CF_pmaa	14	4	2	4
Growth_CNTs	0	9	6	0
Oxygen_species	2	5	14	4
Pristine	2	0	5	17
Ranger tuned (mtry = 3)				
CF_pmaa	13	3	2	4
Growth_CNTs	0	9	6	0
Oxygen_species	2	6	14	4
Pristine	3	0	5	17
Rpart tuned maxdepth				
CF_pmaa	12	1	3	4
Growth_CNTs	0	**13**	7	1
Oxygen_species	1	2	13	3
Pristine	5	2	4	17
Trees with bagging (nbag = 25)				
CF_pmaa	13	2	2	6
Growth_CNTs	0	12	6	0
Oxygen_species	2	3	11	2
Pristine	3	1	8	17
Trees with bagging (nbag = 5000)				
CF_pmaa	**15**	2	2	7
Growth_CNTs	0	10	6	1

(*continued on next page*)

Table A.4 (*continued*)

	CF_pmaa	Growth_CNTs	Oxygen_species	Pristine
Oxygen_species	1	5	13	1
Pristine	2	1	6	16
Trees with bagging (repeated CV)				
CF_pmaa	14	2	2	6
Growth_CNTs	0	8	7	1
Oxygen_species	1	7	14	1
Pristine	3	1	4	17
C5.0 boosting (10 trials)				
CF_pmaa	13	3	2	7
Growth_CNTs	1	12	6	1
Oxygen_species	2	3	13	2
Pristine	2	0	6	15
C5.0 boosting (25 trials)				
CF_pmaa	14	2	2	7
Growth_CNTs	0	12	6	1
Oxygen_species	2	1	12	1
pristine	2	3	7	16
C5.0 boosting (75 trials)				
CF_pmaa	14	2	2	7
Growth_CNTs	0	11	6	2
Oxygen_species	2	2	13	1
Pristine	2	3	6	15
C5.0 boosting (25 trials) – cost penalized				
CF_pmaa	12	2	2	6
Growth_CNTs	0	11	7	1
Oxygen_species	2	3	13	2
Pristine	4	2	5	16
C5.0 boosting (tuned, CV)				
CF_pmaa	14	2	2	7
Growth_CNTs	0	11	6	2
Oxygen_species	2	2	13	1
Pristine	2	3	6	15
AdaBoost				
CF_pmaa	13	3	2	6
Growth_CNTs	0	10	7	0
Oxygen_species	1	4	**15**	4
Pristine	4	1	3	15
Stochastic Gradient Boosting				
CF_pmaa	13	3	2	3
Growth_CNTs	0	9	6	0
Oxygen_species	2	5	14	4
Pristine	3	1	5	**18**
XGBoost				
CF_pmaa	11	3	2	7
Growth_CNTs	0	11	6	1
Oxygen_species	3	4	13	3
Pristine	4	0	6	14
XGBoost (with gamma, 10,000 rounds)				
CF_pmaa	13	2	2	5
Growth_CNTs	0	12	5	2
Oxygen_species	2	3	**15**	2
Pristine	3	1	5	16
XGBoost (with gamma, 100,000 rounds)				
CF_pmaa	13	2	2	5
Growth_CNTs	0	12	5	2
Oxygen_species	2	4	**15**	2
Pristine	3	0	5	16

Table A.5
Prediction metrics of classification tree algorithms on test data.

	RF				RF tuning (Kappa)			
	CF_pmaa	Growth_CNTs	Oxygen_species	Pristine	CF_pmaa	Growth_CNTs	Oxygen_species	Pristine
Accuracy	0.625				0.602			
Precision	**0.833**	**0.778**	0.444	0.556	0.778	0.444	**0.556**	0.640
Recall	0.577	0.519	0.667	0.577	0.519	**0.667**	0.577	0.696
F1	0.682	0.622	0.533	0.566	0.622	0.533	0.566	0.667
MacroAvgPrecision	0.638				0.604			
MacroAvgRecall	0.629				0.614			
MacroAvgF1	0.625				0.597			
MicroAvgPrecision	0.625				0.602			
MicroAvgRecall	0.625				0.602			
MicroAvgF1	0.625				0.602			
	RF tuning (accuracy)				rFerns (tuned)			
	CF_pmaa	Growth_CNTs	Oxygen_species	Pristine	CF_pmaa	Growth_CNTs	Oxygen_species	Pristine
Accuracy	0.602				0.614			
Precision	0.778	0.444	**0.556**	0.640	0.778	0.667	0.519	0.560
Recall	0.519	**0.667**	0.577	0.696	0.519	0.500	0.700	**0.824**
F1	0.622	0.533	0.566	0.667	0.622	0.571	0.596	0.667
MacroAvgPrecision	0.604				0.631			
MacroAvgRecall	0.614				0.636			
MacroAvgF1	0.597				0.614			
MicroAvgPrecision	0.602				0.614			
MicroAvgRecall	0.602				0.614			
MicroAvgF1	0.602				0.614			
	Ranger tuned (mtry = 4)				Ranger tuned (mtry = 3)			
	CF_pmaa	Growth_CNTs	Oxygen_species	Pristine	CF_pmaa	Growth_CNTs	Oxygen_species	Pristine
Accuracy	0.614				0.602			
Precision	0.778	0.500	0.519	0.680	0.722	0.500	0.519	0.680
Recall	0.583	0.600	0.560	0.708	0.591	0.600	0.538	0.680
F1	0.667	0.545	0.538	0.694	0.650	0.545	0.528	0.680
MacroAvgPrecision	0.619				0.605			
MacroAvgRecall	0.613				0.602			
MacroAvgF1	0.611				0.601			
MicroAvgPrecision	0.614				0.602			
MicroAvgRecall	0.614				0.602			
MicroAvgF1	0.614				0.602			
	Rpart tuned maxdepth				Trees with bagging (nbag = 25)			
	CF_pmaa	Growth_CNTs	Oxygen_species	Pristine	CF_pmaa	Growth_CNTs	Oxygen_species	Pristine
Accuracy	0.625				0.602			
Precision	0.667	0.722	0.481	0.680	0.722	0.667	0.407	0.680
Recall	0.600	0.619	0.684	0.607	0.565	**0.667**	0.611	0.586
F1	0.632	0.667	0.565	0.642	0.634	0.667	0.489	0.630
MacroAvgPrecision	0.638				0.619			
MacroAvgRecall	0.628				0.607			
MacroAvgF1	0.626				0.605			
MicroAvgPrecision	0.625				0.602			
MicroAvgRecall	0.625				0.602			
MicroAvgF1	0.625				0.602			
	Trees with bagging (nbag = 5000)				Trees with bagging (repeated CV)			
	CF_pmaa	Growth_CNTs	Oxygen_species	Pristine	CF_ pmaa	Growth_CNTs	Oxygen_species	Pristine
Accuracy	0.614				0.602			
Precision	**0.833**	0.556	0.481	0.640	0.778	0.444	0.519	0.680
Recall	0.577	0.588	0.650	0.640	0.583	0.500	0.609	0.680
F1	0.682	0.571	0.553	0.640	0.667	0.471	0.560	0.680
MacroAvgPrecision	0.628				0.605			
MacroAvgRecall	0.614				0.593			
MacroAvgF1	0.612				0.594			
MicroAvgPrecision	0.614				0.602			
MicroAvgRecall	0.614				0.602			
MicroAvgF1	0.614				0.602			

	C5.0 boosting (10 trials)				C5.0 boosting (25 trials)			
	CF_ pmaa	Growth_CNTs	Oxygen_species	Pristine	CF_pmaa	Growth_CNTs	Oxygen_species	Pristine
Accuracy	0.602				0.614			
Precision	0.722	0.667	0.481	0.600	0.778	0.667	0.444	0.640
Recall	0.520	0.600	0.650	0.652	0.560	0.632	**0.750**	0.571
F1	0.605	0.632	0.553	0.625	0.651	0.649	0.558	0.604
MacroAvgPrecision	0.618				0.632			
MacroAvgRecall	0.606				0.628			
MacroAvgF1	0.604				0.615			
MicroAvgPrecision	0.602				0.614			
MicroAvgRecall	0.602				0.614			
MicroAvgF1	0.602				0.614			

	C5.0 boosting (75 trials)				C5.0 boosting (25 trials) – cost penalized			
	CF_pmaa	Growth_CNTs	Oxygen_species	Pristine	CF_pmaa	Growth_CNTs	Oxygen_species	Pristine
Accuracy	0.602				0.591			
Precision	0.778	0.611	0.481	0.600	0.667	0.611	0.481	0.640
Recall	0.560	0.579	0.722	0.577	0.545	0.579	0.650	0.593
F1	0.651	0.595	0.578	0.588	0.600	0.595	0.553	0.615
MacroAvgPrecision	0.618				0.600			
MacroAvgRecall	0.610				0.592			
MacroAvgF1	0.603				0.591			
MicroAvgPrecision	0.602				0.591			
MicroAvgRecall	0.602				0.591			
MicroAvgF1	0.602				0.591			

	C5.0 boosting (tuned, CV)				AdaBoost			
	CF_pmaa	Growth_CNTs	Oxygen_species	Pristine	CF_pmaa	Growth_CNTs	Oxygen_species	Pristine
Accuracy	0.602				0.602			
Precision	0.778	0.611	0.481	0.600	0.722	0.556	**0.556**	0.600
Recall	0.560	0.579	0.722	0.577	0.542	0.588	0.625	0.652
F1	0.651	0.595	0.578	0.588	0.619	0.571	0.588	0.625
MacroAvgPrecision	0.618				0.608			
MacroAvgRecall	0.610				0.602			
MacroAvgF1	0.603				0.601			
MicroAvgPrecision	0.602				0.602			
MicroAvgRecall	0.602				0.602			
MicroAvgF1	0.602				0.602			

	Stochastic Gradient Boosting				XGBoost			
	CF_pmaa	Growth_CNTs	Oxygen_species	Pristine	CF_pmaa	Growth_CNTs	Oxygen_species	Pristine
Accuracy	0.614				0.557			
Precision	0.722	0.500	0.519	**0.720**	0.611	0.611	0.481	0.560
Recall	**0.619**	0.600	0.560	0.667	0.478	0.611	0.565	0.583
F1	0.667	0.545	0.538	0.692	0.537	0.611	0.520	0.571
MacroAvgPrecision	0.615				0.566			
MacroAvgRecall	0.611				0.559			
MacroAvgF1	0.611				0.560			
MicroAvgPrecision	0.614				0.557			
MicroAvgRecall	0.614				0.557			
MicroAvgF1	0.614				0.557			

	XGBoost (with gamma, 10,000 rounds)				XGBoost (with gamma, 100,000 rounds) elapsed time: 84 min			
	CF_pmaa	Growth_CNTs	Oxygen_species	Pristine	CF_pmaa	Growth_CNTs	Oxygen_species	Pristine
Accuracy	**0.636**				**0.636**			
Precision	0.722	0.667	**0.556**	0.640	0.722	0.667	**0.556**	0.640
Recall	0.591	0.632	0.682	0.640	0.591	0.632	0.652	0.667
F1	0.650	0.649	0.612	0.640	**0.650**	**0.649**	**0.600**	**0.653**
MacroAvgPrecision	0.646				0.646			
MacroAvgRecall	0.636				0.635			
MacroAvgF1	0.638				0.638			
MicroAvgPrecision	0.636				0.636			
MicroAvgRecall	0.636				0.636			
MicroAvgF1	0.636				0.636			

Table A.6
Confusion Matrix of test data by the implementation of 4 SVM algorithms.

	CF_pmaa	Growth_CNTs	Oxygen_species	Pristine
Radial kernel				
CF_pmaa	13	2	2	5
Growth_CNTs	0	**12**	6	1
Oxygen_species	1	4	16	1
Pristine	4	0	3	18
Polynomial kernel				
CF_pmaa	**16**	1	3	5
Growth_CNTs	0	10	7	1
Oxygen_species	0	6	14	1
Pristine	2	1	3	18
Gaussian kernel (Sigma = 3)				
CF_pmaa	13	3	2	4
Growth_CNTs	0	9	2	0
Oxygen_species	2	4	**17**	3
Pristine	3	2	6	18
Gaussian kernel (Sigma = 4)				
CF_pmaa	13	3	2	4
Growth_CNTs	0	9	3	0
Oxygen_species	2	5	16	2
Pristine	3	1	6	**19**

Table A.7
Prediction metrics of 4 SVM algorithms on test data.

	Radial kernel Elapsed time: 2.3 min				Polynomial kernel			
	CF_pmaa	Growth_CNTs	Oxygen_species	Pristine	CF_pmaa	Growth_CNTs	Oxygen_species	Pristine
Accuracy	**0.670**				0.659			
Precision	0.722	**0.667**	0.593	0.720	**0.889**	0.556	0.519	**0.720**
Recall	0.591	0.632	0.727	0.720	**0.640**	0.556	0.667	0.750
F1	**0.650**	**0.649**	**0.653**	**0.720**	0.744	0.556	0.583	0.735
MacroAvgPrecision	0.675				0.671			
MacroAvgRecall	0.667				0.653			
MacroAvgF1	0.668				0.654			
MicroAvgPrecision	0.670				0.659			
MicroAvgRecall	0.670				0.659			
MicroAvgF1	0.670				0.659			
	Gaussian kernel (Sigma = 3)				Gaussian kernel (Sigma = 4)			
	CF_pmaa	Growth_CNTs	Oxygen_species	Pristine	CF_pmaa	Growth_CNTs	Oxygen_species	Pristine
Accuracy	0.648				0.648			
Precision	0.722	0.500	**0.630**	0.720	0.722	0.500	0.593	**0.760**
Recall	0.591	**0.818**	0.654	0.621	0.591	**0.750**	0.640	0.655
F1	0.650	0.621	0.642	0.667	0.650	0.600	0.615	0.704
MacroAvgPrecision	0.643				0.644			
MacroAvgRecall	0.671				0.659			
MacroAvgF1	0.645				0.642			
MicroAvgPrecision	0.648				0.648			
MicroAvgRecall	0.648				0.648			
MicroAvgF1	0.648				0.648			

References

[1] I. Garcia-Moreno, M.A. Caminero, G.P. Rodriguez, J.J. Lopez-Cela, Effect of thermal ageing on the impact damage resistance and tolerance of carbon-fibre-reinforced epoxy laminates, Polymers (Basel) 11 (1) (2019).

[2] M. Hardiman, T.J. Vaughan, C.T. McCarthy, A review of key developments and pertinent issues in nanoindentation testing of fibre reinforced plastic microstructures, Compos. Struct. 180 (2017) 782–798.

[3] C. Xiao, Y. Tan, X. Wang, L. Gao, L. Wang, Z. Qi, Study on interfacial and mechanical improvement of carbon fiber/epoxy composites by depositing multi-walled carbon nanotubes on fibers, Chem. Phys. Lett. 703 (2018) 8–16.

[4] B.C. Ray, D. Rathore, Durability and integrity studies of environmentally conditioned interfaces in fibrous polymeric composites: critical concepts and comments, Adv. Colloid Interf. Sci. 209 (2014) 68–83.

[5] Y.-F. Niu, Y. Yang, S. Gao, J.-W. Yao, Mechanical mapping of the interphase in carbon fiber reinforced poly(ether-ether-ketone) composites using peak force atomic force microscopy: interphase shrinkage under coupled ultraviolet and hydro-thermal exposure, Polym. Test. 55 (2016) 257–260.

[6] D.P. Cole, T.C. Henry, F. Gardea, R.A. Haynes, Interphase mechanical behavior of carbon fiber reinforced polymer exposed to cyclic loading, Compos. Sci. Technol. 151 (2017) 202–210.

[7] Y.-F. Niu, Y. Yang, X.-R. Wang, Investigation of the interphase structures and properties of carbon fiber reinforced polymer composites exposed to hydrothermal treatments using peak force quantitative nanomechanics technique, Polym. Compos. 39 (S2) (2018) E791–E796.

[8] J. Sun, F. Zhao, Y. Yao, Z. Jin, X. Liu, Y. Huang, High efficient and continuous surface modification of carbon fibers with improved tensile strength and interfacial adhesion, Appl. Surf. Sci. 412 (2017) 424–435.

[9] D. Semitekolos, P. Kainourgios, C. Jones, A. Rana, E.P. Koumoulos, C.A. Charitidis, Advanced carbon fibre composites via poly methacrylic acid surface treatment; surface analysis and mechanical properties investigation, Compos. Part B 155 (2018) 237–243.
[10] P. Kainourgios, I.A. Kartsonakis, D.A. Dragatogiannis, E.P. Koumoulos, P. Goulis, C.A. Charitidis, Electrochemical surface functionalization of carbon fibers for chemical affinity improvement with epoxy resins, Appl. Surf. Sci. 416 (2017) 593–604.
[11] S. Termine, A.-F.A. Trompeta, D.A. Dragatogiannis, C.A. Charitidis, Novel CNTs Grafting on Carbon Fibres Through CVD: Investigation of Epoxy Matrix/Fibre Interface Via Nanoindentation 9th EASN International Conference on "Innovation in Aviation & Space", Athens, Greece, 2019.
[12] N.I. Khan, S. Halder, S. Das, J. Wang, Exfoliation level of aggregated graphitic nanoplatelets by oxidation followed by silanization on controlling mechanical and nanomechanical performance of hybrid CFRP composites, Compos. Part B 173 (2019), 106855.
[13] K.T. Butler, D.W. Davies, H. Cartwright, O. Isayev, A. Walsh, Machine learning for molecular and materials science, Nature 559 (2018) 547–555.
[14] A.G. Kusne, T. Gao, A. Mehta, L. Ke, M.C. Nguyen, K.M. Ho, V. Antropov, C.Z. Wang, M.J. Kramer, C. Long, I. Takeuchi, On-the-fly machine-learning for high-throughput experiments: search for rare-earth-free permanent magnets, Sci. Rep. 4 (2014) 6367.
[15] N. Romanos, M. Kalogerini, E.P. Koumoulos, A.K. Morozinis, M. Sebastiani, C. Charitidis, Innovative data management in advanced characterization: implications for materials design, Mater. Today Commun. 20 (2019), 100541.
[16] B. Ribeiro, Support vector machines for quality monitoring in a plastic injection molding process, IEEE Trans. Syst. Man Cybern. Part C Appl. Rev. 35 (3) (2005) 401–410.
[17] P. Larrañaga, D. Atienza, J. Diaz-Rozo, A. Ogbechie, C.E. Puerto-Santana, C. Bielza, Industrial Applications of Machine Learning, 1st ed. CRC Press, 2018.
[18] G. Bolelli, M.G. Righi, M.Z. Mughal, R. Moscatelli, O. Ligabue, N. Antolotti, M. Sebastiani, L. Lusvarghi, E. Bemporad, Damage progression in thermal barrier coating systems during thermal cycling: a nano-mechanical assessment, Mater. Des. 166 (2019), 107615.
[19] B. Vignesh, W.C. Oliver, G.S. Kumar, P.S. Phani, Critical assessment of high speed nanoindentation mapping technique and data deconvolution on thermal barrier coatings, Mater. Des. 181 (2019), 108084.
[20] S.S. Bangaru, C. Wang, M. Hassan, H.W. Jeon, T. Ayiluri, Estimation of the degree of hydration of concrete through automated machine learning based microstructure analysis – a study on effect of image magnification, Adv. Eng. Inform. 42 (2019), 100975.
[21] E.D. Hintsala, U. Hangen, D.D. Stauffer, High-throughput nanoindentation for statistical and spatial property determination, Jom 70 (4) (2018) 494–503.
[22] S. Gautham, S. Sasmal, Recent advances in evaluation of intrinsic mechanical properties of cementitious composites using nanoindentation technique, Constr. Build. Mater. 223 (2019) 883–897.
[23] F.E. Bock, R.C. Aydin, C.J. Cyron, N. Huber, S.R. Kalidindi, B. Klusemann, A review of the application of machine learning and data mining approaches in continuum materials mechanics, Front. Mater. 6 (2019).
[24] E.P. Koumoulos, S.A.M. Tofail, C. Silien, D. De Felicis, R. Moscatelli, D.A. Dragatogiannis, E. Bemporad, M. Sebastiani, C.A. Charitidis, Metrology and nanomechanical tests for nano-manufacturing and nano-bio interface: challenges & future perspectives, Mater. Des. 137 (2018) 446–462.
[25] P.P. Angelov, X. Gu, Empirical Approach to Machine Learning, Springer Nature Switzerland AG, Switzerland, 2019.
[26] A. Panesar, Machine Learning and AI for Healthcare, Apress, Coventry, UK, 2019.
[27] N. Dey, S. Wagh, P.N. Mahalle, M.S. Pathan, Applied Machine Learning for Smart Data Analysis, 1st ed. CRC Press/Taylor & Francis Group, New York, NY, 2019.
[28] P. Sudharshan Phani, W.C. Oliver, A critical assessment of the effect of indentation spacing on the measurement of hardness and modulus using instrumented indentation testing, Mater. Des. 164 (2019), 107563.
[29] K. Ramasubramanian, A. Singh, Machine Learning Using R: With Time Series and Industry-based Use Cases in R, 2nd ed. SpringerLink, 2019.
[30] D. Zhang, L. Qian, B. Mao, C. Huang, B. Huang, Y. Si, A data-driven design for fault detection of wind turbines using random forests and XGboost, IEEE Access 6 (2018) 21020–21031.
[31] V.A. Dev, M.R. Eden, Formation lithology classification using scalable gradient boosted decision trees, Comput. Chem. Eng. 128 (2019) 392–404.
[32] B. Lantz, Machine Learning With R - Third Edition, 3rd ed. Packt Publishing Ltd, Birmingham, 2019.
[33] B. Gupta, Q.Z. Sheng, Machine Learning for Computer and Cyber Security: Principles, Algorithms, and Practices, Taylor & Francis Group, Boca Raton, FL, 2019.
[34] Y. Li, P. Wang, Z. Wang, Evaluation of elastic modulus of cement paste corroded in bring solution with advanced homogenization method, Constr. Build. Mater. 157 (2017) 600–609.
[35] Y. Li, G. Zhang, Z. Wang, P. Wang, Z. Guan, Integrated experimental-computational approach for evaluating elastic modulus of cement paste corroded in brine solution on microscale, Constr. Build. Mater. 162 (2018) 459–469.
[36] E.P. Koumoulos, P. Jagadale, A. Lorenzi, A. Tagliaferro, C.A. Charitidis, Evaluation of surface properties of epoxy–nanodiamonds composites, Compos. Part B 80 (2015) 27–36.
[37] M. Sebastiani, R. Moscatelli, F. Ridi, P. Baglioni, F. Carassiti, High-resolution high-speed nanoindentation mapping of cement pastes: unravelling the effect of microstructure on the mechanical properties of hydrated phases, Mater. Des. 97 (2016) 372–380.
[38] E. Koumoulos, C. Charitidis, Integrity of carbon-fibre epoxy composites through a nanomechanical mapping protocol towards quality assurance, Fibers 6 (4) (2018) 78.
[39] E.P. Koumoulos, K. Paraskevoudis, C.A. Charitidis, Constituents phase reconstruction through applied machine learning in nanoindentation mapping data of mortar surface, J. Compos. Sci. 3 (3) (2019) 63.
[40] E.P. Koumoulos, P. Kainourios, C.A. Charitidis, Assessing the integrity of CFRPs through nanomechanical mapping: the effect of CF surface modification, MATEC Web of Conferences 188 (2018) 01006.
[41] M. Hardiman, T.J. Vaughan, C.T. McCarthy, Fibrous composite matrix characterisation using nanoindentation: the effect of fibre constraint and the evolution from bulk to in-situ matrix properties, Compos. A: Appl. Sci. Manuf. 68 (2015) 296–303.
[42] N.X. Randall, M. Vandamme, F.-J. Ulm, Nanoindentation analysis as a two-dimensional tool for mapping the mechanical properties of complex surfaces, J. Mater. Res. 24 (3) (2011) 679–690.
[43] N.X. Randall, M. Vandamme, F.-J. Ulm, Nanoindentation analysis as a two-dimensional tool for mapping the mechanical properties of complex surfaces, J. Mater. Res. 24 (3) (2011) 679–690.
[44] A. Dey, A. Mukhopadhyay, Nanoindentation of Brittle Solids, CRC Press, Boca Raton, 2014.
[45] M. Tzimas, J. Michopoulos, G. Po, A.C.E. Reid, S. Papanikolaou, Inference and prediction of nanoindentation response in FCC crystals: methods and discrete dislocation simulation examples, Condens. Matter (2019)arXiv 2019, arXiv:1910.07587.
[46] V.V. Asch, Macro-and micro-averaged evaluation measures, Technical Report, CLiPS: Antwerpen, Belgium, 2013.
[47] P. Schober, C. Boer, L.A. Schwarte, Correlation coefficients: appropriate use and interpretation, Anesth. Analg. 126 (5) (2018) 1763–1768.
[48] K.J. Krakowiak, J.J. Thomas, S. Musso, S. James, A.-T. Akono, F.-J. Ulm, Nano-chemo-mechanical signature of conventional oil-well cement systems: effects of elevated temperature and curing time, Cem. Concr. Res. 67 (2015) 103–121.
[49] J.-T. Chien, Source Separation and Machine Learning, Academic Press, 2019.
[50] J. Schmidt, M.R.G. Marques, S. Botti, M.A.L. Marques, Recent advances and applications of machine learning in solid-state materials science, NPJ Comput. Mater. 5 (1) (2019).
[51] F. Buontempo, Genetic Algorithms for Machine Learning, the Pragmatic Programmers, LLC, Raleigh, North Carolina, 2019.